## Supplementary information

### Experimental

*Chemicals and handling*

All chemicals were purchased and used as received in reagent grade. The manipulations were made under air conditions. The products were filtered over the ashless paper and fritted glass with porosity no. 4.

*Physical Measurements*

Elemental analyses were measured by Flash 2000 CHNS apparatus (Thermo Scientific). The samples for FT-IR (ATR) measurements was not dried prior to its using and were used as freshly growth crystals. The Nujol´s absorption UV-Vis spectra (190 - 1100 nm) for solid samples were measured by Specord 250 Plus (Analytica Jena) with the DAD detector at room temperature. Melting points were studied with thermo-microscopy by Kofler hot-stage microscope at 4°C·min$^{-1}$ and reported without corrections.

*Preparation of complex* $[Fe^{III}(L^{Et})_2Cl]$, **1.**

A 100 cm$^3$ round bottom flask was charged with 3-ethoxysalicylaldehyde (0.68 g, 4.12 mmol), furfurylamine (0.36 cm$^3$, 4.12 mmol) and 20 cm$^3$ of MeOH. The reaction mixture was stirred for 1 hour at 70°C, with the colour change to yellow. $FeCl_3$ (0.33 g, 2.06 mmol) was added once and followed previous steps. Dark green crystals were isolated after four days by the filtration from mother liquid. Note: reaction with $FeCl_2·4H_2O$ gives the same result. Yield: 45 %. Melting point 240-246 °C. FT-IR bands (ATR), ν/cm$^{-1}$: 3118, 2976, 2927, 1623 (s) (C=N),1597, 1556, 1502, 1468 (s), 1448 (s), 1412, 1389, 1327, 1292 (s), 1247 (s), 1219 (s), 1149, 1115, 1078, 1012 (s), 970, 893, 800 (s), 759 (s), 735 (s), 646, 609 (s), 600 (s), 582, 540, 490 (s) (s = strong). *Anal. Calc.* for $C_{28}H_{28}ClFeN_2O_6$ (579.82 g·mol$^{-1}$): C, 58.00; H, 4.87; N, 4.83. Found: C, 58.62; H, 4.97; N, 4.54.

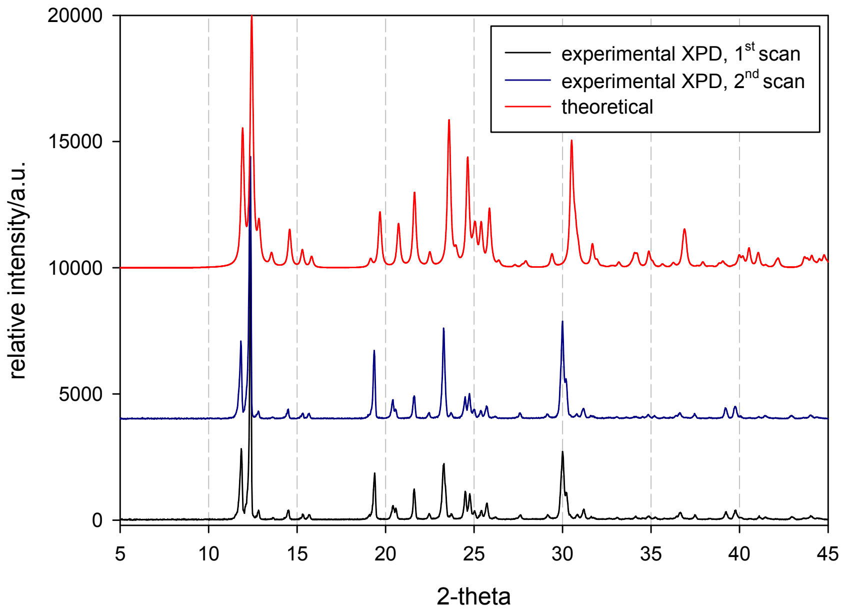

**Figure S1**. Experimental X-ray powder diffraction patterns and theoretical prediction (Mercury software) using the wavelength λ(Co) = 1.78892 Å.

## Spectral data

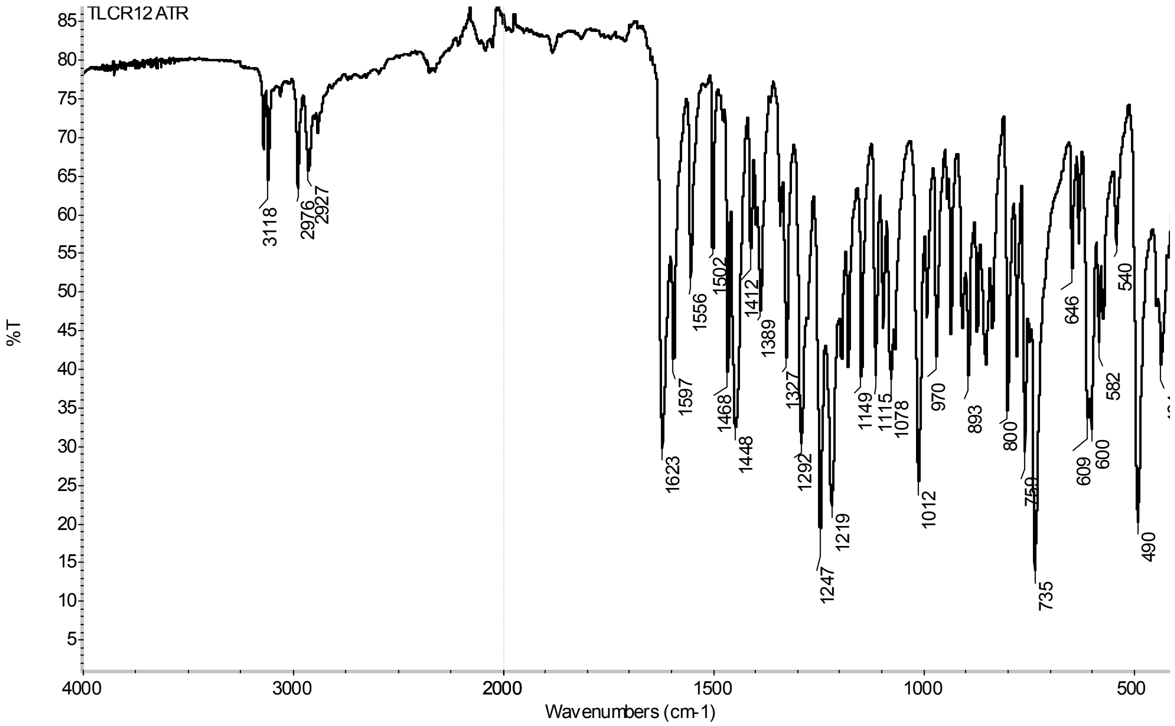

**Figure S2**. IR spectrum of **1**.

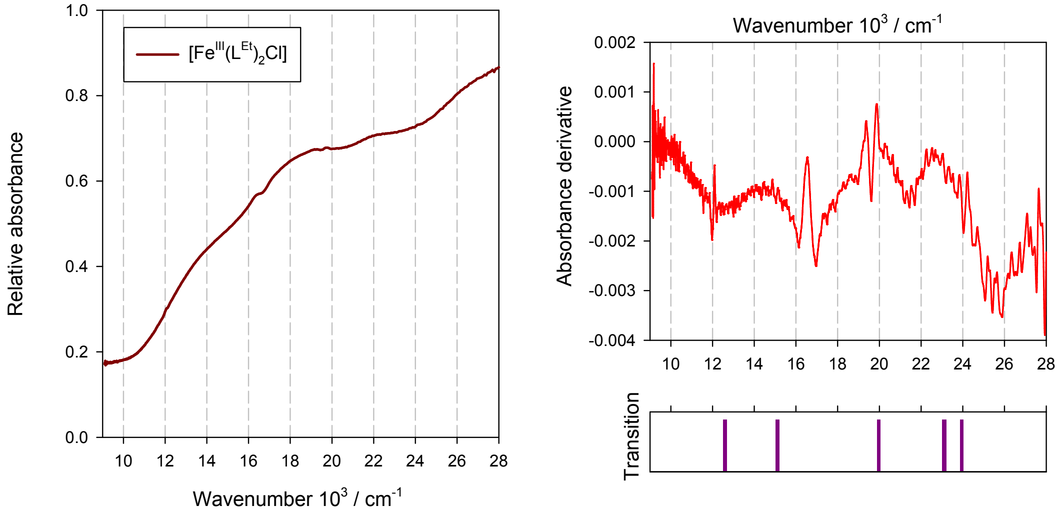

**Figure S3**. Electronic absorption spectrum of **1** in Nujol suspension and its first derivative (right). Vertical bars on right – calculated transitions (spin-orbit corrected excitation energies).

## ***Ab initio* calculations**

**Table S1**. SOC corrected absorption spectrum

```
--------------------------------------------------------------------------------
Multiplets Energy  Wavelength   fosc        T2        |TX|        |TY|       |TZ|
       (cm-1)     (nm)                    (D**2)       (D)         (D)        (D)
--------------------------------------------------------------------------------
 0  6   12582.3    794.8   0.000000001   0.00000   0.00005   0.00000   0.00086
 0  7   12582.3    794.8   0.000000000   0.00000   0.00017   0.00023   0.00030
 0  8   12599.6    793.7   0.000000001   0.00000   0.00013   0.00001   0.00120
 0  9   12599.6    793.7   0.000000001   0.00000   0.00023   0.00044   0.00053
 0 10   15095.9    662.4   0.000000000   0.00000   0.00001   0.00034   0.00040
 0 11   15095.9    662.4   0.000000001   0.00000   0.00004   0.00007   0.00084
 0 12   15120.7    661.3   0.000000003   0.00000   0.00003   0.00141   0.00094
 0 13   15120.7    661.3   0.000000007   0.00001   0.00006   0.00001   0.00245
 0 14   19867.4    503.3   0.000000000   0.00000   0.00004   0.00014   0.00001
 0 15   19867.4    503.3   0.000000000   0.00000   0.00005   0.00000   0.00003
 0 16   23089.0    433.1   0.000000030   0.00002   0.00394   0.00020   0.00093
 0 17   23089.0    433.1   0.000000010   0.00001   0.00168   0.00151   0.00042
 0 18   23142.6    432.1   0.000000017   0.00001   0.00287   0.00060   0.00070
 0 19   23142.6    432.1   0.000000003   0.00000   0.00101   0.00084   0.00025
 0 20   23944.2    417.6   0.000000000   0.00000   0.00039   0.00001   0.00026
 0 21   23944.2    417.6   0.000000000   0.00000   0.00002   0.00003   0.00018
```

**Table S2.** Lowest sextet-to-quartet NEVPT2 transition energies and contributions to the *D*-tensor for **1**

| **Root** | **Multiplicity** | $\Delta E$/cm$^{-1}$ | ***D***/cm$^{-1}$ | ***E***/cm$^{-1}$ |
|---|---|---|---|---|
| 0 | 4 | **12580** | **2.888** | **0** |
| 1 | 4 | **15099** | **-0.932** | **0.932** |
| 2 | 4 | **23135** | **-0.239** | **-0.232** |
| 3 | 4 | **24719** | **-0.019** | **0.018** |
| 5 | 4 | 25843 | 0.002 | 0 |
| 4 | 4 | 26086 | 0.004 | 0 |
| 7 | 4 | 27521 | 0 | 0 |
| 6 | 4 | 28031 | -0.027 | -0.027 |
| 8 | 4 | 28262 | 0 | 0 |
| 9 | 4 | 28812 | -0.082 | 0.070 |
| 10 | 4 | 29904 | 0.081 | -0.003 |
| 12 | 4 | 32077 | -0.675 | -0.665 |
| 13 | 4 | 33148 | 0.002 | 0 |
| 11 | 4 | 33593 | -0.459 | -0.458 |
| 14 | 4 | 33989 | 0 | 0 |
| 15 | 4 | 42148 | -0.684 | 0.681 |
| 16 | 4 | 45579 | 1.250 | 0 |

## Structural data

**Table S3.** Crystal data and structure refinement.

| | $[Fe^{III}(L^{Et})_2Cl]$, **1** |
|---|---|
| Empirical formula | $C_{28}H_{28}ClFeN_2O_6$ |
| Formula weight /g mol$^{-1}$ | 579.82 |
| Crystal system | monoclinic |
| Space group | C2/c |
| Temperature /K | 100 |
| Crystal size /mm | 0.22 × 0.12 × 0.06 |
| $Z$ | 4 |
| $a$ / Å | 16.0599(7) |
| $b$ / Å | 10.4661(3) |
| $c$ / Å | 16.9384(8) |
| $\alpha$ /° | 90 |
| $\beta$ /° | 109.324(3) |
| $\gamma$ /° | 90 |
| $V$ /Å$^3$ | 2686.68(19) |
| $\rho_{calc}$ /g cm$^{-3}$ | 1.433 |
| $\mu$ /mm$^{-1}$ | 5.798 |
| $F$(000) | 1204.0 |
| Radiation | CuK$\alpha$ ($\lambda$ = 1.54186) |
| 2Θ range for data collection/° | 10.272 to 143.21 |
| Index ranges | $-19 \leq h \leq 16$, $-8 \leq k \leq 12$, $-20 \leq l \leq 20$ |
| Data/restraints/parameters | 2584/0/174 |
| Goodness-of-fit on $F^2$ | 1.063 |
| Final R indexes [I>=2σ (I)] | $R_1 = 0.0308$, $wR_2 = 0.0710$ |
| R indices (all data) | $R_1 = 0.0368$, $wR_2 = 0.0744$ |
| color | dark green |
| CCDC No. | 1855298 |

**Table S4**. Selected bond lengths (Å) and bond angles (°) in chromophore $\{FeN_2O_2Cl\}$ of **1.**

| | | | |
|---|---|---|---|
| Fe1–O1 | 1.8792(12) | O11–Fe1–Cl1 | 114.98(4) |
| Fe1–O1$^1$ | 1.8793(12) | O1–Fe1–Cl1 | 114.98(4) |
| Fe1–N1 | 2.1094(15) | O1–Fe1–O11 | 130.04(9) |
| Fe1–N1$^1$ | 2.1093(15) | O1–Fe1–N1 | 86.93(6) |
| Fe1–Cl1 | 2.2339(8) | O11–Fe1–N1 | 89.03(6) |
| | | O11–Fe1–N11 | 86.94(6) |
| | | O1–Fe1–N11 | 89.03(6) |
| | | N1–Fe1–Cl1 | 94.78(4) |
| | | N11–Fe1–Cl1 | 94.78(4) |
| | | N11–Fe1–N1 | 170.43(9) |

**Table S5.** Comparison of geometry for related complexes using SHAPE software.

| Complex | Trigonal bipyramid (TBPY) / $D_{3h}$ | Spherical square pyramid (SPY) / $C_{4v}$ | Ref. |
|---|---|---|---|
| $[Fe^{III}(L^{Et})_2Cl]$ | **0.976** | 2.800 | this work |
| $[Fe^{III}(L^{Me})_2Cl]$ | 3.127 | **1.003** | unpublished |
| $[Fe^{III}(L^2)_2Cl]$ | 2.808 | **0.976** | Ref. * |
| $[Fe^{III}(L^4)_2Cl]$ | **1.978** | **1.717** | Ref. * |

(*) Cisterna, J.; Artigas, V.; Fuentealba, M.; Hamon, P.; Manzur, C.; Hamon, J.-R.; Carrillo, D. Pentacoordinated Chloro-Iron(III) Complexes with Unsymmetrically Substituted N2O2 Quadridentate Schiff-Base Ligands: Syntheses, Structures, Magnetic and Redox Properties. *Inorganics* **2018**, *6*, 5.

## Description of crystal structure

The crystal structure of **1** (**Figure S4**) show C–H···Cl hydrogen bonding interactions between carbon atoms (C10) of furane ring and chlorine atoms (Cl1) [C10–H10···Cl1 with distance C10···Cl1 of 3.522(2) Å (**Table S6**)], C–H···O hydrogen bonding interactions between carbon atoms (C12) of furane ring and fenolic oxygen atoms (O1) [C12–H12···O1 with distance C12···O1 of 3.367(2) Å (**Table S6**)], and also CH/π interactions between methylene carbon atoms (C13) and carbon atoms (C10) of furane ring [C13–H13A···C10 with distance C13···C10 of 3.722(2) Å].

The π-π stacking interaction[4] have been observed in crystal structure. The π-π stacking interactions in **1** is observed between two benzene rings [C1–C6] with $C_g\cdots C_g$ distance of 3.65 Å, and shift distance of 1.46 Å (**Figure S5**).

## Hirshfeld surface analysis

The characterization using Hirshfeld surface and Fingerprint plots were made through the program CrystalExplorer17.5.[1-3] The surface was shown transparent to allow clear viewing of molecules and the crystal interaction environment. The fingerprint plots were displayed in the standard 0.4–3.0 Å for axes scale $d_e$ and $d_i$. The Hirchfeld surface surrounded a molecule is defined by points where the attempt to the electron density from the molecule of interest is equal to the contribution from all the other molecules. The 3D Hirshfeld surface mapped over the normalizes contact distances ($d_{norm}$) of **1** is illustrated in **Fig. S6**. The 3D Hirshfeld surfaces of **1** mapped over shape index is drawn in **Fig. S7**. The surface is shown as transparent to allow visualization of molecules, around which they were calculated. The 3D surface mapped over $d_{norm}$ represents the circular depressions (deep red) visible on the Hirshfeld surface indicative of C–H···O, C–H···Cl and C–H···π contacts. Other visible spots in the Hirchfeld surfaces correspond to H···H contacts. The Hirchfeld surface plotted over shape index visualize π-π interactions in **1** (**Fig. S7**).

Hirshfeld 2D fingerprint plots allow a quick and easy identification of the significant intermolecular interactions map on the molecular surface.[5,6] As shown in **Fig. S8**, the weak H···O/O···H hydrogen bonding interactions represent 16.8%, of the total Hirshfeld surface with two distinct spikes in the 2D fingerprint plots, indicating hydrogen bonding interactions are the most significant interaction in the crystal. The analysis Hirshfeld 2D fingerprint plots of **1** shows weak H···Cl/Cl···H hydrogen bonding interactions in proportion 9.2%, and weak H···C/C···H hydrogen bonding interactions in proportion 22.5%, (**Fig. S8**). The scattered points in the fingerprint plots illustrate proportion of C···C interactions (3.5%) and H···H interactions (46.7%) of the total Hirshfeld surface.

(1) (a) Hirchfeld, F. L. Bonded-atom fragments for describing molecular charge densities. *Theor. Chim. Acta* **1977**, *44*, 129-138; (b) Spackman, M. A.; Jayalitaka, D. Hirshfeld surface analysis. *CrystEngComm* **2009**, *11*, 19-32.

(2) (a) Spackman, M. A.; McKinnon, J. J. Fingerprinting intermolecular interactions in molecular crystals. *CrystEngComm* **2002**, *4*, 378-392; (b) Parkin, A.; Barr, G.; Dong, W.; Gilmore, C. J.; Jayalitaka, D.; McKinnon, J. J.; Spackman, M. A.; Wilson, C. C. Comparing entire crystal structures: structural genetic fingerprinting. *CrystEngComm* **2007**, *9*, 648-652.

(3) Turner, M. J.; McKinnon, J. J.; Wolff, S. K.; Gromwood, D. J.; Spackman, P.R.; Jayalitaka, D.; Spackman, M.A. CrystalExplorer17.5. The University of Western Australia, 2017.

(4) Janiak, C. A critical account on π–π stacking in metal complexes with aromatic nitrogen-containing ligands. *J. Chem. Soc., Dalton Trans.* **2000**, 3885–3896.

(5) McKinnon, J.J.; Spackman, M.A.; Mitchell, A.S. Novel tools for visualizing and exploring intermol-ecular interactions in molecular crystals. *Acta Crystallogr., Sect. B* **2004**, *B60*, 627–668.

(6) McKinnon, J. J.; Jayatilaka, D.; Spackman, M. A. Towards quantitative analysis of intermolecular interactions with Hirshfeld surfaces. *Chem. Commun.* **2007**, 3814–3816.

**Table S6.** Hydrogen bonding interactions parameters of **1**

| D–H···A | Symmetry code | d(D–H) /Å | d(H–A) /Å | d(D–H) /Å | <(D–H–A)/° |
|---|---|---|---|---|---|
| C10–H10···Cl1 | 1/2+x,-1/2+y,+z | 0.95 | 2.89 | 3.522(2) | 125 |
| C7–H7···O2 | | 0.95 | 2.67 | 3.223(2) | 118 |
| C12–H12···O1 | 1/2+x,1/2+y,+z | 0.95 | 2.50 | 3.367(2) | 152 |
| C12–H12···O3 | 1/2+x,1/2+y,+z | 0.95 | 2.72 | 3.437(2) | 132 |

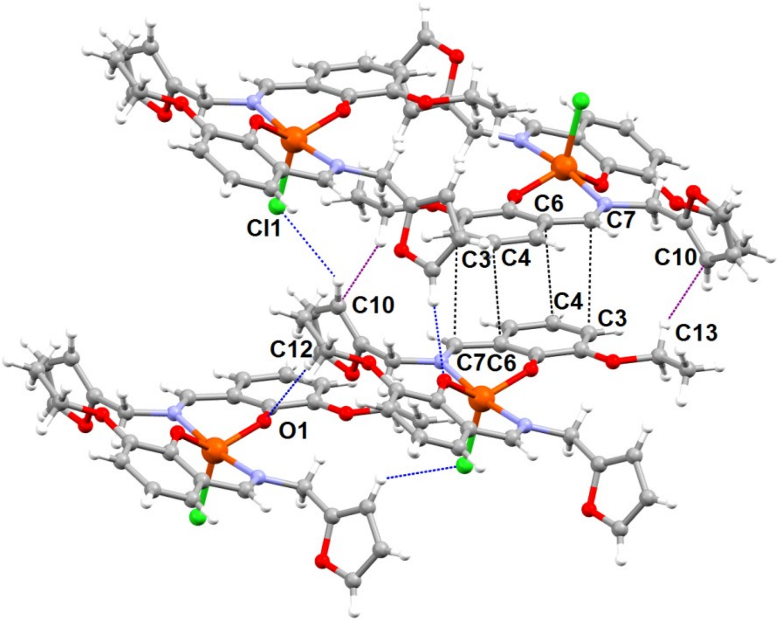

**Figure S4**. The C–H···Cl and C–H···O hydrogen bonds (blue dashed lines), C–H···π hydrogen bonding interactions (violet dashed lines), and π-π stacking interactions (black dashed lines) in crystals structure of **1**.

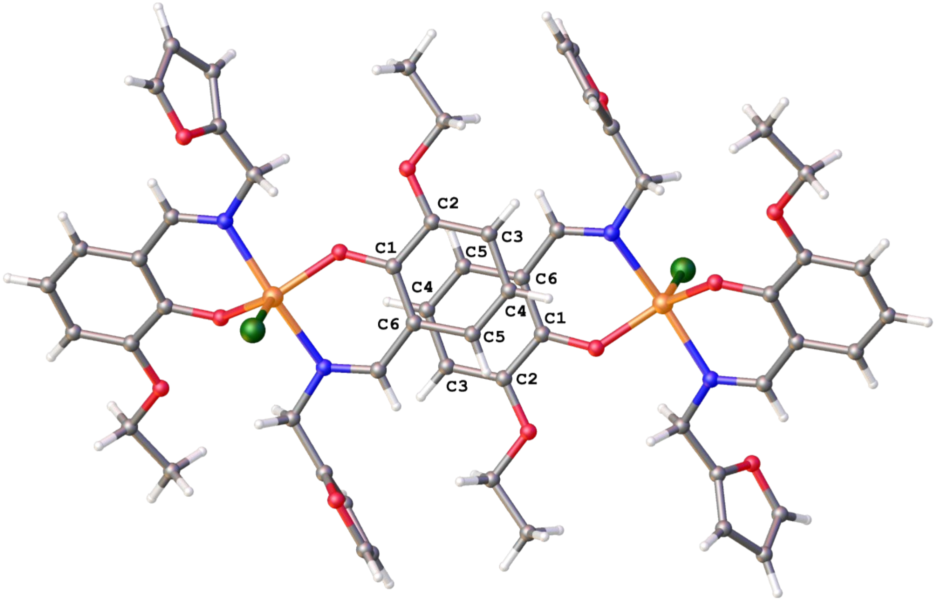

**Figure S5**. The π-π stacking interactions in crystal structure of **1**.

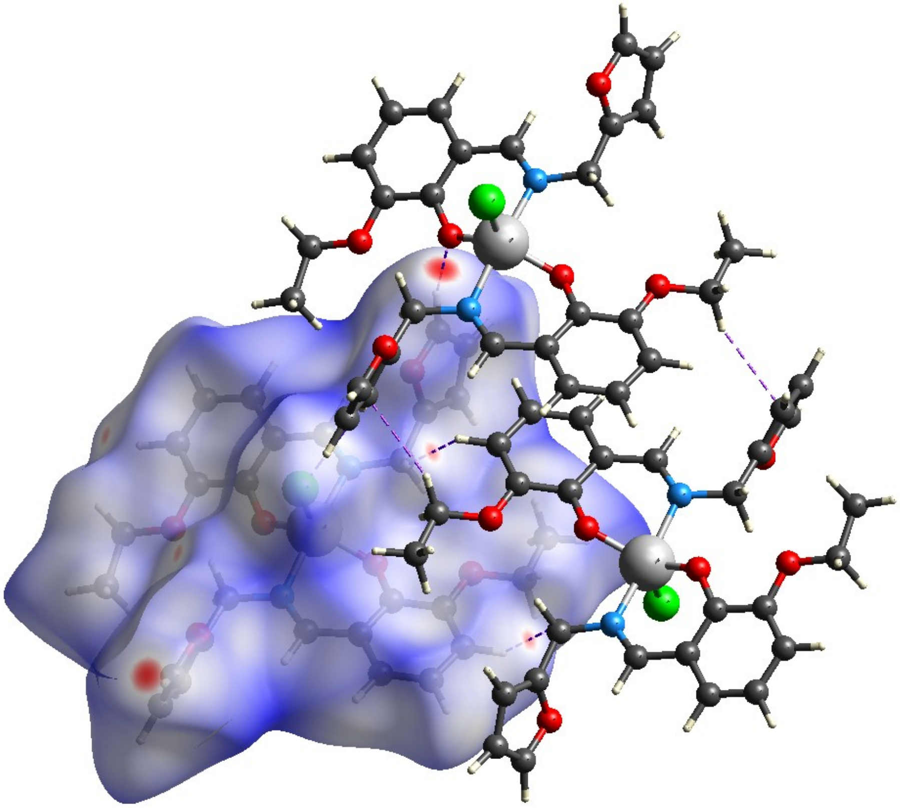

**Figure S6**. View of the three-dimensional Hirshfeld surface of **1** plotted over $d_{\text{norm}}$ in the range -0.1689 to 1.5730 a.u.

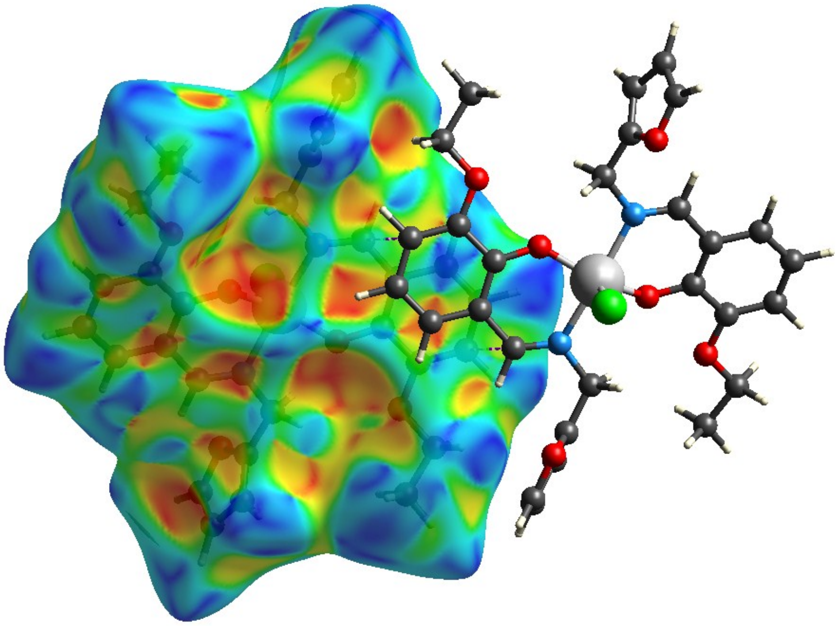

**Figure S7.** View of the three-dimensional Hirshfeld surface of **1** plotted over shape index showing π-π stacking interactions.

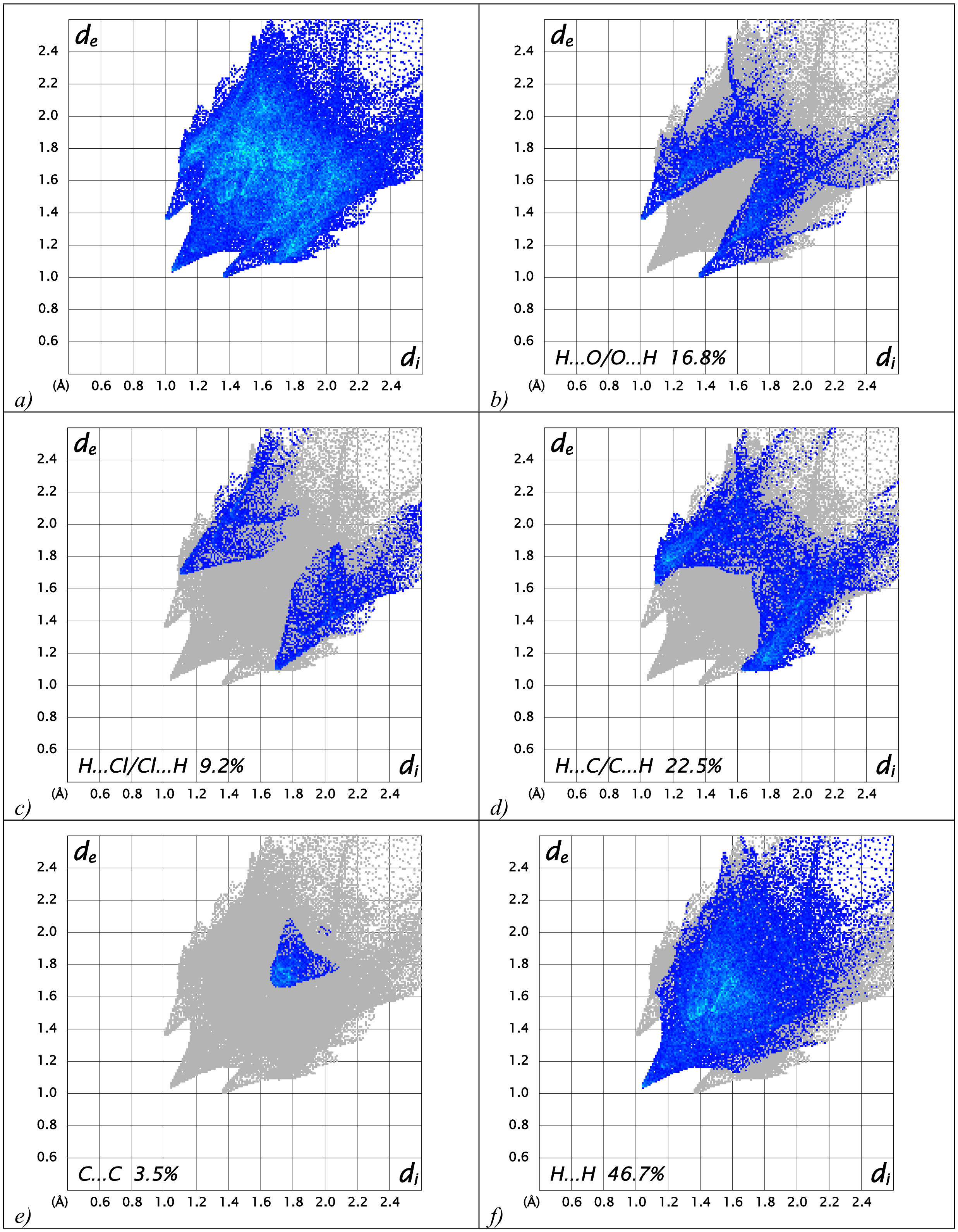

**Figure S8**. The full two-dimensional fingerprint plots of **1**, showing (*a*) all interactions, and delineated into (*b*) H···O/O···H, (*c*) H···Cl/Cl···H, (*d*) H···C/C···H, (*e*) O···O, and (*f*) H···H interactions. The $d_\mathrm{i}$ and $d_\mathrm{e}$ values are the closest internal and external distances from given on the Hirshfeld surface contacts.

**DC magnetic data**

ZFS Hamiltonian: $\hat{H} = D(\hat{S}_z^2 - \hat{S}^2/3)\hbar^{-2} + g_{\mathrm{eff}} B_z \mu_{\mathrm{B}} \hat{S}_z \hbar^{-1}$

a) $D > 0$: $g_{\mathrm{eff}} = 1.97(6)$, $D/hc = +2.0(8)$ cm$^{-1}$, molecular-field correction $zj/hc = -0.011$ cm$^{-1}$, and the overall temperature-independent magnetism $\chi_{\mathrm{TIM}} = -7.4 \times 10^{-9}$ m$^3$ mol$^{-1}$. $E$ parameter – omitted. Discrepancy factors: $R(\chi) = 0.0056$, $R(M) = 0.058$.

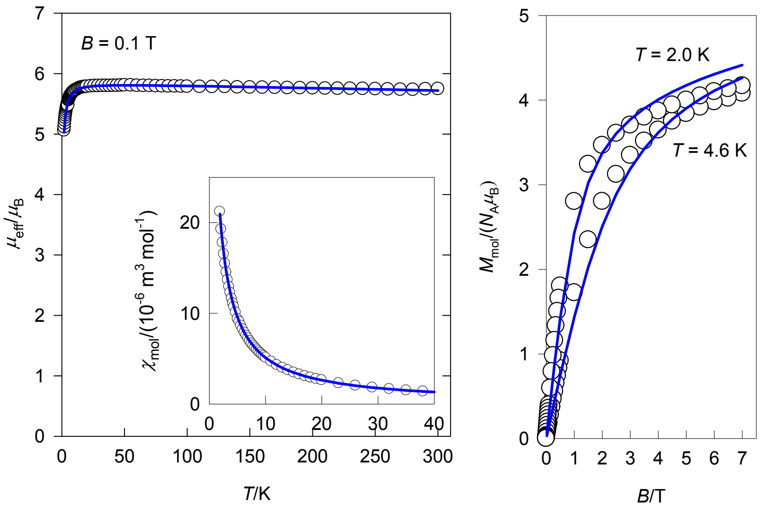

b) $D < 0$: $g_{\mathrm{eff}} = 1.97(4)$, $D/hc = -1.5(4)$ cm$^{-1}$, molecular-field correction $zj/hc = -0.019$ cm$^{-1}$, and the overall temperature-independent magnetism $\chi_{\mathrm{TIM}} = -6.7 \times 10^{-9}$ m$^3$ mol$^{-1}$. $E$ parameter – omitted. Discrepancy factors: $R(\chi) = 0.0044$, $R(M) = 0.071$.

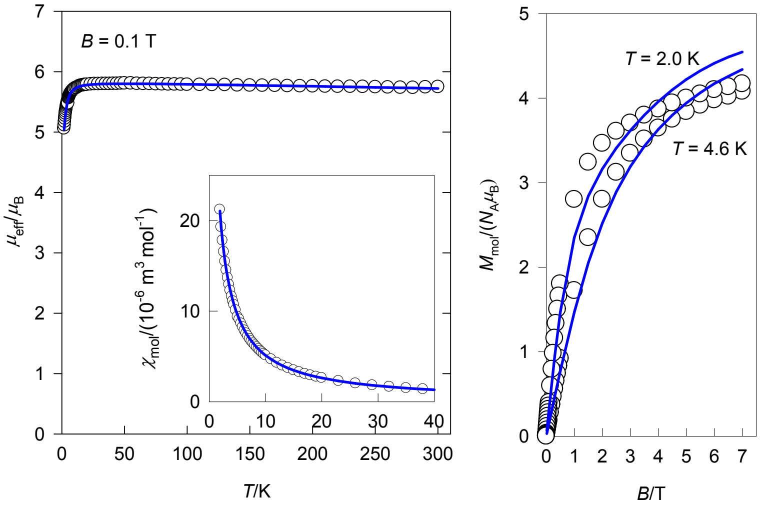

**Figure S9.** Magnetic functions for **1**. Left – temperature dependence of the effective magnetic moment (inset: molar magnetic susceptibility); right – field dependence of the magnetization per formula unit. Lines – fitted using the zfs model.

## AC susceptibility

Fitting of the AC susceptibility data is based upon 44 data points (22 in-phase and 22 out-of-phase) using the formula for the **two-set Debye model**

$$\chi(\omega)=\chi_S+\frac{\chi_{T1}-\chi_S}{1+(\mathrm{i}\omega\tau_1)^{1-\alpha_1}}+\frac{\chi_{T2}-\chi_{T1}}{1+(\mathrm{i}\omega\tau_2)^{1-\alpha_2}} \quad \text{or}$$

$$\chi(\omega)=\chi_S+(\chi_T-\chi_S)\left[\frac{x_1}{1+(\mathrm{i}\omega\tau_1)^{1-\alpha_1}}+\frac{1-x_1}{1+(\mathrm{i}\omega\tau_2)^{1-\alpha_2}}\right]$$

where $x_1$ is the weight of the first, low-frequency relaxation set (channel, branch). This equation decomposes into two explicit formulae for

a) the in-phase component

$$\chi'(\omega)=\chi_S+(\chi_{T1}-\chi_S)\frac{1+(\omega\tau_1)^{1-\alpha_1}\sin(\pi\alpha_1/2)}{1+2(\omega\tau_1)^{1-\alpha_1}\sin(\pi\alpha_1/2)+(\omega\tau_1)^{2-2\alpha_1}}+(\chi_{T2}-\chi_{T1})\frac{1+(\omega\tau_2)^{1-\alpha_2}\sin(\pi\alpha_2/2)}{1+2(\omega\tau_2)^{1-\alpha_2}\sin(\pi\alpha_2/2)+(\omega\tau_2)^{2-2\alpha_2}}$$

b) the out-of-phase component

$$\chi''(\omega)=(\chi_{T1}-\chi_S)\frac{(\omega\tau_1)^{1-\alpha_1}\cos(\pi\alpha_1/2)}{1+2(\omega\tau_1)^{1-\alpha_1}\sin(\pi\alpha_1/2)+(\omega\tau_1)^{2-2\alpha_1}}+(\chi_{T2}-\chi_{T1})\frac{(\omega\tau_2)^{1-\alpha_2}\cos(\pi\alpha_2/2)}{1+2(\omega\tau_2)^{1-\alpha_2}\sin(\pi\alpha_2/2)+(\omega\tau_2)^{2-2\alpha_2}}$$

with the constraint for the isothermal susceptibilities $\chi_{T1}<\chi_{T2}$ in order to get positive contributions from each primitive component. Then $x_1=(\chi_{T1}-\chi_S)/(\chi_{T2}-\chi_S)=(\chi_S-\chi_{T1})/(\chi_S-\chi_{T2})$.

Seven free parameters ($\chi_S$, $\chi_{T1}$, $\chi_{T2}$, $\alpha_1$, $\alpha_2$, $\tau_1$, and $\tau_2$) can be fitted reliably by using 44 experimental data points. The functional to be minimized accounts to the relative errors of both susceptibility components

- $F=w\cdot E(\chi')+(1-w)\cdot E(\chi'')$ with the typical weight $w = 0.07$, or
- $F=E(\chi')\cdot E(\chi'')$ with $E(\chi)=(1/N)\left[\sum_i^N\left|(\chi_i^{\mathrm{e}}-\chi_i^{\mathrm{c}})/\chi_i^{\mathrm{e}}\right|\right]$

The extension to the three-set Debye model is straightforward.

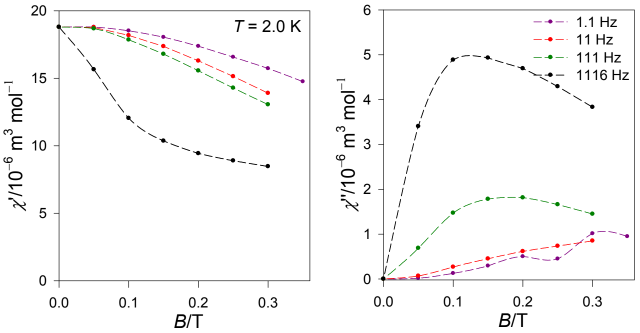

**Figure S10.** AC susceptibility data for **1**: field dependence for a set of frequencies at $T = 2.0$ K.

**Table S7**. Field dependence of AC susceptibility parameters for **1** at $T = 1.9$ K. [a]

| $B_{DC}$/T | $R(\chi')$ /% | $R(\chi'')$ /% | $\chi_S$ | $\chi_{LF}$ | $\alpha_{LF}$ | $\tau_{LF}$ / $10^{-3}$ s | $\chi_{IF}$ | $\alpha_{IF}$ | $\tau_{IF}$ /$10^{-3}$ s | $\chi_{HF}$ | $\alpha_{HF}$ | $\tau_{HF}$ /$10^{-6}$ s | $x_{LF}$ | $x_{IF}$ | $x_{HF}$ |
|---|---|---|---|---|---|---|---|---|---|---|---|---|---|---|---|
| 0.15 | 0.41 | 2.3 | 4.8(2) | 5.6(3) | .00 | **671(152)** | 6.6(2) | .01 | 42(8) | 19.7(1) | .14(1) | 232(4) | .05 | .07 | .88 |
| 0.30 | 0.31 | 1.5 | 3.0(1) | 4.2(4) | .02 | **506(97)** | 7.2(2) | .11(4) | 58(6) | 17.7(1) | .21(1) | 178(3) | .08 | .12 | .71 |
| 0.45 | 1.0 | 2.8 | 2.6(6) | 3.9(9) | .00 | **640(205)** | 8.1(6) | .16(6) | 73(17) | 15.4(2) | .25(4) | 111(15) | .11 | .33 | .57 |
| 0.60 | 0.74 | 3.2 | | 1.9(6) | .00 | **618(90)** | 5.4(1) | .13(4) | 75(12) | 13.0(1) | .39(2) | 29(1) | .15 | .27 | .58 |
| 0.75 | 1.1 | 5.7 | | 1.9(7) | .00 | **525(100)** | 4.5(1) | .10(7) | 71(17) | 10.5(1) | .45(4) | 12(2) | .19 | .25 | .57 |
| 0.90 | 1.8 | 13 | | 1.6 | .00 | **350(229)** | 3.5(3) | .16 | 75 | 8.4(1) | .49(15) | 4.3(29) | .19 | .23 | .58 |
| 1.05 | 2.6 | 11 | | 1.4(9) | .00 | **506(201)** | 2.8(2) | .01 | 73(32) | 6.9(2) | .60(14) | 1.4(17) | .20 | .19 | .60 |
| 1.20 | 2.7 | 15 | | 1.0(4) | .00 | **414(136)** | 2.0(2) | .01 | 72(31) | 5.6(1) | .60(21) | 0.6(14) | .18 | .17 | .65 |

[a] Obtained by a three-set Debye model; $\chi$ in units of $10^{-6}$ m$^3$ mol$^{-1}$.

$$x_{\mathrm{LF}} = (\chi_{T,\mathrm{LF}} - \chi_S)/(\chi_T - \chi_S),\ x_{\mathrm{IF}} = (\chi_{T,\mathrm{IF}} - \chi_{T,\mathrm{LF}})/(\chi_T - \chi_S),\ x_{\mathrm{HF}} = (\chi_{T,\mathrm{HF}} - \chi_{T,\mathrm{IF}})/(\chi_T - \chi_S),\ \chi_{T,\mathrm{HF}} = \chi_T$$

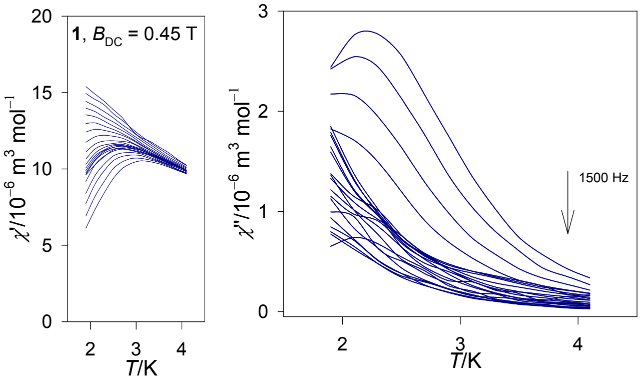

**Figure S11.** Temperature evolution of the AC susceptibility components for different frequencies ranging between $f = 0.1$ to 1500 Hz.

**Table S8**. Temperature dependence of AC susceptibility parameters for **1** at $B_{DC} = 0.45$ T.

| $T$/K | $R(\chi')$ /% | $R(\chi'')$ /% | $\chi_S$ | $\chi_{LF}$ | $\alpha_{LF}$ | $\tau_{LF}$ / $10^{-3}$ s | $\chi_{IF}$ | $\alpha_{IF}$ | $\tau_{IF}$ /$10^{-3}$ s | $\chi_{HF}$ | $\alpha_{HF}$ | $\tau_{HF}$ /$10^{-6}$ s | $x_{LF}$ | $x_{IF}$ | $x_{HF}$ |
|---|---|---|---|---|---|---|---|---|---|---|---|---|---|---|---|
| 1.9 | 1.0 | 2.8 | 2.6(6) | 3.9(9) | .00 | 640(205) | 8.1(6) | .16(6) | 73(17) | 15.4(2) | .25(4) | 111(15) | .11 | .33 | .57 |
| 2.1 | 0.56 | 2.8 | 3.3(4) | 4.9(11) | .15 | 739(299) | 7.9(5) | .20(7) | 67(20) | 15.3(2) | .19(3) | 95(8) | .14 | .25 | .61 |
| 2.3 | 0.41 | 2.8 | 3.3(4) | 4.7(5) | .02 | 777(104) | 7.0(5) | .18(5) | 65(12) | 14.7(1) | .17(2) | 66(6) | .12 | .20 | .68 |
| 2.5 | 0.52 | 1.9 | 3.7(7) | 5.4(16) | .25 | 788(583) | 6.7(8) | .19(16) | 63(43) | 14.3(4) | .17(3) | 51(8) | .16 | .12 | .72 |
| 2.7 | 0.36 | 2.4 | 3.7(8) | 4.9(12) | .23 | 787(479) | 5.9(9) | .19(14) | 66(42) | 13.7(2) | .18(3) | 35(6) | .13 | .10 | .78 |
| 2.9 | 0.42 | 2.2 | 3.7 | 4.3(6) | .00 | 730(235) | 5.3(1) | .27(13) | 96(93) | 12.9(1) | .18(2) | 24(1) | .06 | .11 | .83 |
| 3.1 | 0.50 | 2.5 | 3.7 | 4.4(5) | .04 | 714(224) | 4.9(1) | .21(20) | 70(73) | 12.4(1) | .20(2) | 17(1) | .08 | .06 | .86 |
| 3.3 | 0.27 | 2.8 | 3.7 | 4.3(2) | .00 | 608(84) | 4.6(1) | .18(18) | 56(39) | 11.9(1) | .24(2) | 10.7(6) | .08 | .04 | .89 |
| 3.5 | 0.28 | 3.0 | 3.7 | 4.2(8) | .01 | 590(87) | 4.5(2) | .40 | [91] | 11.5(1) | .27(4) | 6.7(7) | .07 | .03 | .90 |
| 3.7 | 0.31 | 4.0 | 3.7 | 4.2(4) | .00 | 617(152) | 4.3(1) | .29 | [74] | 11.1(1) | .30(4) | 4.2(7) | .06 | .02 | .91 |
| 3.7 | 0.43 | 5.5 | 3,7 | 4.3(1) | .12(6) | 523(72) | | | | 11.1(1) | .38(3) | 3.1(5) | .08 | - | .92 |
| 3.9 | 0.29 | 6.5 | 3.7 | 4.2(1) | .08(5) | 544(56) | | | | 10.7(1) | .41(2) | 1.9(3) | .07 | - | .93 |
| 4.1 | 0.27 | 5.2 | 3.7 | 4.1(1) | .06(6) | 527(54) | | | | 10.3(1) | .43(2) | 1.1(2) | .06 | - | .94 |

[a] Obtained by a three-set (two-set) Debye model; $\chi$ in units of $10^{-6}$ m$^3$ mol$^{-1}$.